Metabolic imaging detects low levels of glycolytic activity that vary with levels of c-Myc expression in patient-derived xenograft models of glioblastoma

Richard Mair[1, 2, 3], Alan Wright[1, 3], Susana Ros[1, 3], De-en Hu[1, 3], Tom Booth[1, 3], Felix Kreis[1, 3], Jyotsna Rao[1], Colin Watts[2, 3], Kevin M. Brindle[1, 3, 4]

1. Cancer Research UK Cambridge Institute, University of Cambridge, Cambridge, UK
2. Division of Neurosurgery, Department of Clinical Neurosciences, University of Cambridge, Cambridge, UK
3. Cancer Research UK Major Centre - Cambridge, Cancer Research UK Cambridge Institute, Cambridge, UK
4. Department of Biochemistry, University of Cambridge, Cambridge UK.

Running title: Metabolic imaging of c-Myc expression in glioblastoma models

Abbreviations: GB, glioblastoma; HK2, hexokinase 2; LDHA, lactate dehydrogenase A; MCT, monocarboxylate transporter; MRSI, magnetic resonance spectroscopic imaging; PDOX, patient-derived orthotopically implanted xenograft; 5-ALA, 5-aminolevulinic acid; GB4 c-myc KD, GB4 cells expressing a doxycycline-inducible shRNA targeting c-Myc; LPR, hyperpolarized [1-^{13}C]lactate/[1-^{13}C]pyruvate signal ratio

Financial support: The work was supported by a Cancer Research UK Programme grant (17242) and by the CRUK-EPSRC Imaging Centre in Cambridge and Manchester (16465) awarded to K. M. Brindle. F. Kreis was supported by a Marie Curie ITN studentship (EUROPOL) and R. Mair by Addenbrooke's Charitable Trust and a CRUK Cambridge Centre Fellowship.

Corresponding author: Kevin Michael Brindle, Cancer Research UK Cambridge Institute, University of Cambridge, Li Ka Shing Centre, Robinson Way, Cambridge CB2 0RE, UK. Email: kmb1001@cam.ac.uk

Declaration of competing financial interests:

The hyperpolarizer is on loan from GE Healthcare (GEH) and is the subject of a research agreement between the University of Cambridge, Cancer Research UK and GE Healthcare. KMB holds patents with GEH on some aspects of DNP technology.

Statement of Significance: Metabolic imaging with hyperpolarized [1-^{13}C]pyruvate detects low levels of c-Myc-driven glycolysis in patient-derived glioblastoma models which, when translated to the clinic, could be used to detect occult disease, determine disease prognosis, and target radiotherapy.

Abstract

^{13}C magnetic resonance imaging (MRI) of hyperpolarized [1-^{13}C]pyruvate metabolism has been used in oncology to detect disease, investigate disease progression, and monitor response to treatment with a view to guiding treatment in individual patients. This technique has translated to the clinic with initial studies in prostate cancer. Here we use the technique to investigate its potential uses in patients with glioblastoma (GB). We assessed the metabolism of hyperpolarized [1-^{13}C]pyruvate in an orthotopically implanted cell line model (U87) of GB and in patient-derived tumors, where these were produced by orthotopic implantation of cells derived from different patients. Lactate labeling was higher in the U87 tumor when compared to patient-derived tumors, which displayed inter-tumoral heterogeneity, reflecting the intra- and inter-tumoral heterogeneity in the patients' tumors from which they were derived. Labeling in some patient-derived tumors could be observed before their appearance in morphological images, while in other tumors it was not significantly greater than the surrounding brain. Increased lactate labeling in tumors correlated with c-Myc driven expression of hexokinase 2 (HK2), lactate dehydrogenase A (LDHA) and the monocarboxylate transporters (MCT) and was accompanied by increased radio-resistance. Since c-Myc expression correlates with glioma grade, this study demonstrates that imaging with hyperpolarized [1-^{13}C]pyruvate could be used clinically with GB patients to determine disease prognosis, to detect early responses to drugs that modulate c-Myc expression and to select tumors, and regions of tumors, for increased radiotherapy dose.

Introduction

Gliomas represent 80% of primary tumors affecting the adult human central nervous system and are classified into four types. The most aggressive, grade IV glioblastoma (GB), accounts for more than 50% of all diagnosed adult gliomas (1,2). De-bulking surgery followed by radiotherapy with concomitant administration of temozolomide is the current standard of care treatment (3), however median survival is only 15 months (4). The tumor is driven by multiple genetic alterations, including loss of the phosphatase and tensin homolog (PTEN) gene, amplification of the epidermal growth factor receptor (EGFR), and increased signaling via the phosphatidylinositol-3-kinase (PI3K)/Akt pathway (2,5). The latter pathway is activated in more than 88% of cases, which results in up-regulated glucose transporter expression and increased glycolysis and is associated with tumor progression and resistance to treatment (6,7). Expression of the transcription factor c-Myc is correlated with glioma grade and between 60–80% of GB exhibit elevated levels of Myc (8,9). Myc also drives increased expression of the glycolytic enzymes in order to meet the elevated biosynthetic demands of increased cell proliferation (10).

Hyperpolarization of ^{13}C-labeled metabolites, which can increase their sensitivity to magnetic resonance detection by more than 10,000x (11), has revolutionized our capability to image metabolism in vivo (12) and has already translated to the clinic (13). Previous ^{13}C magnetic resonance spectroscopic imaging (MRSI) studies of hyperpolarized [1-^{13}C]pyruvate metabolism in orthotopically implanted cell line models of GB have shown much higher levels of labeled lactate in the tumor when compared to surrounding normal

brain tissue (14). The purpose of this study was to determine whether this was also the case in patient-derived orthotopically implanted xenograft (PDOX) models of GB, which more faithfully reproduce the biology of patient tumors than the cell line models (15,16), and to determine whether there were differences in pyruvate metabolism between PDOX models derived from different patients.

Materials and Methods

Assessment of intra-tumoral heterogeneity in patient tumors by fluorescence-guided multi-region sampling. Intra-operative sampling of 4 patients with confirmed GB was performed by an experienced neurosurgeon (CW). Cytoreductive surgery was guided by giving the patients 5-aminolevulinic acid (5-ALA) 6 hours prior to surgery (17). Tissue sampling was performed using a Zeiss OPMI Pentero operating microscope (Zeiss, Welwyn Garden City, UK) for fluorescence detection of protoporphyrin IX (a 5-ALA metabolite) (Zeiss) (18). Written informed consent was obtained from the patients, the studies were conducted in accordance with the Declaration of Helsinki and were approved by an institutional review board.

Cell culture. Brain tumor tissue was collected from GB patients using protocols compliant with the UK Human Tissue Act 2004 (HTA licence ref 12315), approved by the Local Regional Ethics Committee (LREC ref 04/Q0108/60) and in accordance with the Declaration of Helsinki. Informed consent was obtained from each patient. Tumor tissue was disaggregated in

phosphate-buffered saline (PBS) and cells isolated by filtration through a 40 µm filter (Falcon, UK) and washed with 10 mL red blood cell lysis buffer (Abcam, UK). Cell viability was assessed by Trypan blue dye exclusion and viable cells were seeded at 15,000 cells cm^2 and grown as monolayer cultures on extracellular matrix (ECM)-coated T_{75} flasks (Engelbreth-Holm-Swarm murine sarcoma ECM gel – 1:10 dilution, Sigma, UK) in phenol red-free Neurobasal A (Gibco, UK) medium containing 20 mM L-glutamine (Sigma, UK), 1% Streptomycin/Penicillin/Amphotericin B (Invitrogen, UK), 20 ng/mL hEGF (Sigma, UK), 20 ng/mL hFGF (R&D systems, UK), 2% B27 (Invitrogen, UK) and 1% N2 (Invitrogen, UK). U87 cells (American Tissue Culture Collection, Manassas, US) were grown in Dulbecco's modified Eagle's medium (DMEM) supplemented with 2 mM L-glutamine and 10% fetal bovine serum (Gibco, UK). Cell line authentication was performed using STR genotyping contemporaneously with the experiments. Cells were used within 3 passages of being thawed. Mycoplasma testing was performed using RNA-capture ELISA.

Generation of cell lines expressing doxycycline-inducible shRNA targeting c-Myc. Short hairpin (sh)RNA sequences targeting c-MYC were cloned into the doxycycline-inducible TetOnPLKO lentiviral vector (Addgene) (19,20) using the following oligonucleotides:

shMYC seq F:

5'-

CCGGCCTGAGACAGATCAGCAACAACTCGAGTTGTTGCTGATCTGTCTC

AGGTTTTTG

shMYC seq R:

5’ –

AATTCAAAAACCTGAGACAGATCAGCAACAACTCGAGTTGTTGCTGATCT

GTCTCAGG

The control sequences were:

shCtrl F:

5’-

CCGGCCTAAGGTTAAGTCGCCCTCGCTCGAGCGAGGGCGACTTAACCTT

AGG

shCtrl R:

5’ -

AATTCCTAAGGTTAAGTCGCCCTCGCTCGAGCGAGGGCGACTTAACCTT

AGG

Lentiviruses were produced by co-transfecting HEK 293T cells with the shRNA plasmid and the packaging plasmids pCMVΔR8.91 (gag-pol) and pMD.G (VSV-G glycoprotein) (21). Supernatants containing lentiviruses were collected 72 h after transfection, mixed with polybrene (8 μg/ml) and used to infect GB4 cells. Fresh medium containing puromycin (2 μg/ml) was added after 24 h and cells were selected for at least 48 h.

c-Myc knock down. Transduced GB4 cells were grown in 6 well plates to approximately 50% confluency in serum-free medium. Cells were then incubated with doxycycline (10 ng/mL) for 48 h in serum-free medium, harvested and protein extracted for western blot analysis to confirm knock down of c-Myc and determine the concentrations of LDHA and HK2.

Orthotopic tumor model. Procedures were performed in compliance with project and personal licenses issued under the United Kingdom Animals (Scientific Procedures) Act, 1986 and were approved by the Cancer Research UK, Cambridge Institute Animal Welfare and Ethical Review Body. Tumors were created by intracranial implantation of cells in 6 week-old (200-250 g) female rnu/rnu athymic nude rats (Charles River, Germany; Harlan, UK). Cells, below passage 20, were counted and assessed for viability (Vi-CELL XR, Beckman Coulter, Brea, US) before re-suspension in culture media at 2 x 10^6 cells μL^{-1}. Animals were anaesthetized by inhalation of 1-2% isoflurane (Isoflo, Abbotts Laboratories Ltd., UK) in O_2 (flow rate 2 L min^{-1}). Analgesia, administered subcutaneously (Vetergesic (Alstoe, York, UK), contained 0.3 mg/mL buprenorphine hydrochloride and 0.135% w/v chlorocresol diluted 1:10 in 0.9% sodium chloride, and 1 mL/kg of subcutaneous Rimadyl LA (Pfizer, New York, US) containing carpofen (Zoetis, Florham Park, NJ, US) (5 mg/kg diluted 1: 10 in 0.9% sodium chloride). Animals were placed in a stereotactic surgical frame (Kopf, Tujunga, US) and a 1 mm hole drilled 2 mm anterior and 3 mm lateral to the bregma (right-side). Five µL of the cell suspension were delivered 6 mm intracranially via a 23-gauge full displacement syringe (SGE Analytical Science, Melbourne, Australia).

Magnetic Resonance Imaging. MR experiments were performed using a 7T spectrometer (Agilent, Palo Alto, US). Animals were anesthetized following inhalation of 1-2% isoflurane in O_2 (flow rate 2 L min^{-1}) and core body temperature, breathing and heart rate were monitored (SA instruments Inc.,

Stonybrook, US). Axial ^{1}H MR (T_2-weighted) images were acquired using a 72 mm inner-diameter ^{1}H quadrature birdcage coil (Rapid Biomedical GMBH, Rimpar, Germany) and a fast spin-echo pulse sequence (TR, 1500 ms; TE, 40 ms across a matrix of 256 x 256 data points with a field of view (FOV) of 40 x 40 mm and 4-8 averages). Slice thickness was 2 mm and 15 contiguous slices were obtained. Contrast agent-enhanced images were acquired using a T_1-weighted spoiled-gradient-echo sequence prior to and then 90 seconds after injection of 100 µmol/kg Dotarem (Guebert). Images consisted of 5 slices 1.5 mm thick with gaps of 0.3 mm centered on the tumor with TR 43 ms, TE 4.6 ms, 27° flip angle and 4 averages. The field of view was 40 mm x 40 mm with a 256 x 128 data matrix.

Proton magnetic resonance spectroscopy. Lactate spectra were acquired from single 4 x 4 x 4 mm voxels using LASER acquisition (22) and VAPOR water suppression (23) pulse sequences and the 72 mm diameter volume coil for transmit and a quadrature coil placed over the rat's head for receive (Rapid Biomedical, Rimpar, Germany). Spectra were acquired with echo times (TE) of 37 and 144 ms and 512 averages, or 1024 averages for the longer TE. In one tumor an extra spectrum was acquired with TE 288 ms and 1024 averages. Water reference spectra were acquired at a TE of 37 ms and using 16 averages. Spectral regions between 1 and 1.6 ppm was least-squares fitted to a model of a lactate methyl resonance doublet, at all three echo times, and a broad lipid methylene resonance at TE=37 ms. This fitting was also used to calculate the lactate methyl resonance T_2. The water T_2 was measured using STEAM localization, using 16 TE values between 0.005 and

0.50 seconds and 16 averages. The lactate methyl and water T_2s were used to estimate their respective intensities at TE=0. Assuming a tissue water concentration of 46 M (24), these intensities were used to estimate a lactate concentration. Similar water and lactate spectra were acquired from 6 x 8 x 4 mm voxels in normal brain; 512 averages at TE=37 ms and 1024 at TE=144 s for the lactate spectra and 16 averages at TE=37 ms for the water spectra. The same T_2 value for lactate and a mean value for the water T_2 in the tumors were used for concentration calculations. Data were processed in MATLAB (Mathworks, Natick, USA).

Dynamic nuclear hyperpolarization. [1-^{13}C]pyruvic acid (82 mg) containing 15 mM trityl radical, tris(8-carboxy2,2,6,6-tetra-(hydroxyethyl)-benzo-[1,2-4,50]-bis-(1,3)-dithiole-4-yl)-methyl sodium salt (OXO63; both GE Healthcare) was mixed with 1.5 mM of gadoterate meglumine (Guerbet) and polarized as described previously (25). After dissolution this gave a 184 mM hyperpolarized [1-^{13}C]pyruvate solution at room temperature with a pH of 7.2 and between 17 and 21% polarization.

^{13}C magnetic resonance spectroscopic imaging. ^{13}C spectroscopic images were acquired using a 20 mm diameter transmit/receive surface coil (Varian, Palo Alto, US) inside the 72 mm diameter ^{1}H volume coil and positioned under the supine rat head. T_2-weighted ^{1}H images were used to define a 6 mm slice that incorporated the maximum dimensions of the tumor. A slice-selective shim was then performed. Hyperpolarized [1-^{13}C]pyruvate was injected via a tail vein cannula, which took approximately 10 s. Single

time point axial ^{13}C chemical shift images were obtained from the 6 mm slice, where image acquisition started 20 s after pyruvate injection (TR 30 ms; TE 1.2 ms; FOV 40 x 40mm; data matrix 32 x 32; sinc excitation pulse with approximate 5º flip angle at 13 mm from the surface coil; spectral width 6010 Hz; acquisition time 21.3 ms; 128 complex data point pairs; with phase-encoding gradients preceding signal acquisition). Lactate-to-pyruvate ratios were calculated using an in-house MATLAB script. Voxels were included if the signal was 3.5 times the standard deviation determined from 100 voxels in noise regions, and if there was an adjacent voxel that met this criterion. Areas under the peaks were calculated by time domain fitting of the resonances after spatial Fourier transformation. Animals implanted with GB4 c-myc KD cells were imaged when tumors were >0.1 cm^3. They were then fed a doxycycline diet for 1 week and re-imaged (Doxycycline diet, 0.2 g/kg food pellet, Harlan D.98186).

Determination of sensitivity to radiotherapy. GB1 and GB4 cell lines were grown in duplicate to 50% confluence and then treated with a single dose (15 Gy) of radiotherapy using a Cs-137 irradiator (IBL 637; CIS Bio International, Saclay, France). Cell viability was determined using an automated Trypan blue dye exclusion assay (ViCell, Beckman Coulter, US) at 1, 3, 5 and 7 days after irradiation.

GB4 control cells, which included non-transduced cells and cells transduced with a lentivral vector expressing a doxycycline-inducible control shRNA, and GB4 cells expressing a doxycycline-inducible shRNA targeting c-Myc (GB4 c-

myc KD) were grown to approximately 50% confluence in serum-free media. They were then treated with either doxycycline (10 ng/mL) alone or doxycycline (10 ng/mL) for 48 h before treatment with a single dose of 15 Gy and cell viability determined.

GB4 tumor-bearing rats were treated 24 h after imaging with hyperpolarized [1-^{13}C]pyruvate. Rats were anaesthetized using inhalation anesthesia and a lead collimator was used to protect the snout and body. Animals were wrapped in insulating plastic and silver foil to maintain body temperature and Lubrithal (Dechra, Leakwood, US) was applied for eye protection. For low dose therapy Temozolomide (100 mg kg^{-1}) was dissolved in 1 mL water and administered by oral gavage 1 hour prior to radiotherapy. Radiotherapy (15 Gy) was delivered over 825 s using a Cs-137 irradiator (IBL 637; CIS Bio International, Saclay, France). The Temozolomide dose was split so that 50 mg kg^{-1} was given 1 hour prior to the first fraction of radiotherapy (15 Gy) and also 1 hour prior to the second fraction (15 Gy) 72 h later. A further 10 Gy radiation dose was given at 72 h later giving a total of 40 Gy and 100 mg kg^{-1} of Temozolomide.

Histopathology and immunohistochemistry. Brains were excised and immediately placed in 10% formalin (Sigma-Aldrich, St Louis, US) for 24 h, then in 70% ethanol and then sectioned. Hematoxylin and eosin staining (H&E) (ST020 Multistainer – Leica Microsystems, Wetzlar, Germany) was performed on 5 μm sections, which were cut using the surface injection site as a guide for the center of the underlying tumor. Further 10 μm sections were

taken for TUNEL staining and immunohistochemistry (IHC). TUNEL was performed using Leica's Polymer Kit (Leica Microsystems, Wetzlar, Germany) and Promega's DeadEnd Colorimetric TUNEL System (Promega, Madison, US). IHC was performed using Leica's Polymer Refine Kit and human-specific antibodies. Specifically; Ki67 – 1:200 dilution (M7240, Dako, Espoo, Finland), Monocarboxylate Transporter (MCT) 1 – 1:500 dilution (HPA003324, Atlas, Stockholm, Sweden), MCT 4 – 1:500 dilution (HPA021451, Atlas, Stockholm, Sweden), Glial Fibrillary Acid Protein (GFAP) – 1:10,000 dilution (Z0334, Dako, Espoo, Finland), c-Myc – 1:50 dilution (ab32072, Abcam, UK), pAKT – 1:25 dilution (3787, Cell Signalling Technology, Danvers, US). Images were analyzed using Aperio image viewing software using in-house algorithms.

Western blotting. Protein was extracted from cell and tissue samples in Pierce RIPA buffer, containing protease inhibitor and EDTA (Thermo Fisher, US). Cell disruption was performed using either sonication (cell culture) (Bioruptor, Diagenode, Liege, Belgium) or via homogenization (tissues) (Precellys, Bertin, Rockville, US). Proteins were separated using gel electrophoresis in NuPage Bis-Tris precast gels (Thermo Fisher, Waltham, US) and dry-blotted onto polyvinylidene difluoride (PVDF) membranes using an iBlot transfer stack (Thermo Fisher, Waltham, US). Subsequent analysis was performed using the Odyssey Licor near-infrared digital fluorescence imaging system (Licor biotechnology, Lincoln, NE, US). Samples were analyzed in duplicate or triplicate and data from technical replicates were averaged. Antibodies were used at manufacturer recommended dilutions: c-Myc – Abcam ab32072 1:10000; pAKT Cell Signalling Technology #9271

1:1000; HK2 – Cell Signalling Technology #2106 1:1000; LDHA – Cell Signalling Technology #3582 1:1000.

Whole exome sequencing. Massively parallel sequencing exome capture was performed using Illumina Nextera Rapid Capture, according to the manufacturer's protocol. Fragment size was confirmed using a Bioanalyser (DNA1000 chip) before pre-capture pooling and qPCR, using the KAPA Quantification Kit, to confirm DNA concentration. Exome sequencing was performed on an Illumina HiSeq 2500 using v4 chemistry generating 125-bp paired-end reads with dual indexing. Variant calling used a pipeline based on Burrows-Wheeler Aligner (BWA). BWA-mem was used for mapping sequencing reads to the human reference genome (GRCh37) (26). The genome analysis toolkit (GATK) (version 3.5) was then used to apply local indel realignment and to recalibrate base quality scores (27). Variant calling was carried out jointly using the GATK HaplotypeCaller. Annotation of variants was accomplished using ANNOVAR(28). Oncotator was used for further annotation of candidate variants with cancer relevant annotations (29).

Statistics. All statistics were performed using GraphPad Prism (GraphPad Software Inc, California, US) and MATLAB (MathWorks, Massachusetts, US).

Results

Patient-derived orthotopic xenografts resemble the human disease

Derivation of the cell lines and the conditions used to culture them have been shown to give GB PDOX models that recapitulate the biology of the

tumors from which they were derived (15,16). The four models studied, originating from four individual GB patients, showed variable growth rates and grew more slowly than the U87 cell line model (30) (**Fig. 1 a**). These models reproduced the morphology of the patient tumors, for example GB4 had a minimally infiltrative margin compared to GB2, in both the patient tumor and corresponding PDOX (**Suppl. Fig 1a**). The models showed high expression of a glial cell marker (GFAP) (31) *in vivo* (**Fig. 1 b**) and a neural stem cell marker (nestin) *in vitro* (15) (**Fig. 1 c**). U87 showed negligible expression of either marker. Exome sequencing showed PTEN frameshift mutations in GB1 – 3 tumors, which resulted in protein loss (**Suppl. Fig. 1 b**), and in GB4 a frameshift (fs) mutation in PIK3R1 (V73fs), which encodes the regulatory protein p85α and that could lead to activation of PI3K (5,32) (**Suppl. Table 1**). Consistent with these observations, all the models showed activation of the PI3K/Akt pathway, as indicated by phosphorylation of Akt (pAkt) (**Suppl. Fig 1 c**).

A patient-derived orthotopic xenograft showed increased lactate labeling when compared to normal brain

^{13}C images of non tumor-bearing animals showed low intensity signals from lactate (**Fig. 1 d**). At 1 month after implantation of GB4 cells the hyperpolarized [1-^{13}C]lactate/[1-^{13}C]pyruvate signal ratio (LPR) increased significantly in the hemisphere containing injected cells (**Fig. 1 e**) compared to the contralateral hemisphere (n=11, *p=0.02, paired t-test) (**Fig. 1f**). There was no difference in non-injected controls (n=6, p=0.9, paired t-test) (**Fig. 1g**). LPR was significantly elevated in the right lower brain quadrant, containing

cells, when compared to the left lower quadrant (**Fig. 1h**) (n=11, *p=0.01, paired t-test). There was no difference in the upper right and left quadrants (**Fig. 1 i**). Since the cell injection needle passed through the upper right quadrant, where there was no change in LPR, the increased LPR in the lower right quadrant could not simply be the result of tissue damage. At this stage no tumor was visible in T_2-weighted ^{1}H MR images of tissue water (**Fig. 1 j**) and there was no signal enhancement in T_1-weighted images following contrast agent injection (**Fig. 1 k,l**).

Tumors derived from different patients showed variable levels of lactate labeling

LPRs measured in tumor-containing regions, identified by hyperintensity on T_2-weighted ^{1}H images, were significantly higher in GB3 and GB4 tumors, whereas GB1 and GB2 tumors showed an LPR similar to normal brain (**Fig. 2**). Images were acquired when tumors were ~0.1 cm^3 or greater. However, GB4 tumors were generally larger than GB1 tumors (*p=0.03, GB4 n=12, GB1 n=5, unpaired t-test) (**Suppl. Fig 1 d**) and therefore to eliminate the potential confounding effect of tumor size on LPR we removed from the analysis all those tumors above a threshold size of 0.35 cm^3. When this was done there was no longer a significant difference in volume between GB1 and GB4 tumors (p=0.3, GB4 n=7, GB1 n=6, unpaired t-test) (**Suppl. Fig 1 e**) but the difference in LPR between GB1 and GB4 was maintained (p=0.001, GB4: n=7, GB1: n=6, unpaired t-test) (**Suppl. Fig 1 f**). The variability in labeling in the GB4 model, although large, is comparable with that observed previously in U87 tumors in mice (33).

Lactate labeling correlated with c-Myc expression

Lactate labeling depends upon pyruvate delivery (34), lactate concentration and the activities of LDH (35) and the monocarboxylate transporters (MCTs) (35,36). Expression of the MCTs and enzymes in the glycolytic pathway, including LDHA and HK2, is driven by c-Myc (10). The concentrations of c-Myc, LDHA and HK2 were higher in GB3 and GB4 tumors, which showed high levels of lactate labeling, than in GB1 and GB2 tumors (**Fig. 3 a-e**). This trend, however, was not repeated in cell culture, where GB3 cells showed lower levels of c-Myc than GB2 but comparable levels of LDHA and HK2 (**Fig. 3 f-h; Suppl. Fig. 2 a-f**). This does not appear to be due to hypoxia since none of the four PDOX models shown here (GB1 – GB4) expressed HIF-1α in vivo (**Suppl. Fig. 2 g**), and only one (GB5), out of the 5 PDOXs studied, expressed HIF-1α in vivo (**Suppl. Fig. 2 g**). None of the cell lines expressed HIF-1α in culture (**Suppl. Fig. 2 h**)). Localized proton spectroscopy measurements gave GB4 tumor lactate concentrations of 2 – 8 mM (n=4), as compared to ≤2 mM in normal rat cortex (n=2), consistent with an association between increased HK2 levels and aerobic glycolysis in glioblastoma (32). Proton spectra of the brains of two of the four GB4 tumor-bearing animals and spectra from the brains of the two non tumor-bearing animals are shown in **Suppl. Fig. 3**. Increased plasma membrane expression of MCTs, a negative prognostic factor in the clinic (37), was observed in tumors with a high LPR (MCT1 in GB3 and GB4 and MCT4 in GB4) (**Fig. 3 i**).

Expression of c-Myc (38) and HK2 (39) have been associated with a worse prognosis. We observed a positive correlation between c-Myc

expression and LPR (n=2 per GB cohort, r^2=0.83, **p=0.0017, linear regression) (**Figure 3 j**), and a correlation, although poorer, between growth rate (**Fig. 1a**) and c-Myc expression (**Figure 3 a,d,e**), with GB1 tumors showing comparable growth rates to GB3 tumors and only slightly lower growth rates than GB4 tumors. However, there was no correlation between tumor growth rate and cell proliferation, as assessed by Ki67 staining, with slower growing GB1 tumors, with low c-Myc expression, showing significantly (p<0.0001) higher levels of Ki67 staining (**Suppl. Fig. 2i**) than faster growing GB4 tumors, with high c-Myc expression. The reasons for this discrepancy between tumor cell proliferation and tumor growth rate are unclear but cannot be explained by higher rates of cell turnover in GB1 tumors since there was no difference in the levels of cell death (TUNEL staining) between untreated GB1 and GB4 tumors (**Suppl. Fig. 2 j**).

Inhibition of the PI3K/Akt pathway has been shown previously to decrease GB lactate labeling in animal models injected with hyperpolarized [1-^{13}C]pyruvate (14). However, here there was a negative correlation between the levels of pAKT and LPR (n=2 per GB cohort, r^2=0.76, p=0.0047) (**Fig 3 k**).

We confirmed that c-Myc-driven expression of LDHA and HK2 was responsible for increased lactate labeling by knocking down c-Myc expression in GB4 cells. Doxycycline treatment of GB4 cells expressing a doxycycline-inducible shRNA targeting c-Myc (GB4 c-Myc KD) substantially decreased c-Myc, LDHA and HK2 expression (**Fig 4 a-c**), and in tumors derived from these cells LPR was decreased at 7 days after addition of doxycycline to the diet of tumor-bearing animals (**Fig. 4 d-f**).

Variable lactate labeling in the tumor models reflects intra- and inter-tumoral heterogeneity in GB patients

Lactate labeling and c-Myc, LDHA, HK2 and MCT expression were reproducible between PDOXs derived from the same patient but different to those derived from other patients. To determine whether this was due to inter- or intratumoral heterogeneity we conducted 5ALA fluorescence-guided multi-region tumor sampling (40) in four GB patients. The levels of c-Myc, HK2 and LDHA varied between 3 – 5 spatially disparate samples (**Suppl. Fig. 4 a-g**), indicating that PDOX heterogeneity reflects patient intra- as well as inter-tumoral heterogeneity. As in the PDOX models, LDHA and HK2 expression was correlated with c-Myc expression (**Suppl. Fig. 4 h,i**) (3-5 regions per tumor, 2 technical replicates per location, r^2=0.30, p=0.036 and r^2=0.27, p=0.048 respectively).

Inhibition of c-Myc expression increased radiosensitivity in cultured cells

Expression of HK2 and LDHA have been negatively correlated with radiosensitivity (39,41), suggesting that metabolic imaging with hyperpolarized [1-^{13}C]pyruvate could be used to target increased radiotherapy dose to areas of radio-resistance. We investigated this by comparing the effects of irradiation on GB4 and GB1 cells. Following irradiation, GB4 cells, which have a high LPR *in vivo* (**Fig. 2f**) and high c-Myc expression *in vitro* and *in vivo* (**Fig. 3 a,d**), showed a greater preservation of viability than GB1 cells (**Fig. 4 g**, p<0.0001), which have a lower LPR *in vivo* (**Fig. 2f**) and lower levels of c-

Myc *in vitro* and *in vivo* (**Fig. 3 a,d**). Doxycycline-induced c-Myc knock down in GB4 cells resulted in a greater decrease in cell viability following irradiation (**Fig. 4 h**). Control cells (non-transduced cells or cells transduced with a control shRNA) showed no significant difference in viability following irradiation in the presence or absence of doxycycline (**Suppl. Fig. 5**).

Radiotherapy results in decreased lactate labeling in GB4 tumors

GB4 tumors responded to radiotherapy and Temozolomide treatment with a decrease in LPR 72 h after treatment ($p=0.038$, $n=6$, paired t-test) (**Fig. 4 i – k**). TUNEL staining of excised tumor sections showed that this was accompanied by significant increases in cell death ($p=0.0089$, $n=11$ untreated $n=8$ treated, unpaired t-test) (**Fig. 4 l**).

Discussion

Studies in human brain tumors and in patient-derived GB xenografts implanted orthotopically in immune-compromised mice have shown that contrary to expectations, where the tumors were expected to be predominantly glycolytic, there was extensive oxidation of glucose in the tricarboxylic acid (TCA) cycle (42,43). In these experiments the patients and mice were infused with ^{13}C-labeled glucose immediately prior to tumor resection and the ^{13}C-labeling patterns in tumor metabolites were analyzed by ^{13}C NMR measurements on tumor extracts. The relatively low levels of lactate labeling observed in the PDOX models used here, which were similar

to those observed in normal brain, are consistent with these previous studies. The much higher levels of lactate labeling observed in the established cell line model used here (U87), and in the GB cell line models used in previous studies with hyperpolarized [1-^{13}C]pyruvate (14), which have been shown to be poor models of human brain tumors (15), reflects presumably their extended lifetime in culture and their very high rates of proliferation rather than being a necessary feature of malignancy. Previous studies with hyperpolarized [1-^{13}C]pyruvate in these cell line models of glioma may, therefore, be overestimating the levels of labeled lactate that are likely to be observed in the clinic. The PDOX models used here, which showed much higher levels of expression of glial (GFAP) and neural stem cell (nestin) markers than the U87 model, are more representative of the human disease.

The patterns of lactate labeling were reproducible between GB PDOXs derived from the same patient but different to those derived from other patients. Multi-region sampling of individual GB patients showed this likely reflected inter and intra-tumoral heterogeneity (40). The relatively low levels of lactate labeling in the PDOXs has important implications for translation of this technique to the clinic since it suggests that some tumors, or some regions of tumors, may show lactate labeling that is indistinguishable from labeling in normal brain. However, the observation of increased lactate labeling in brain regions where no tumor was apparent in a T_2-weighted ^{1}H image of tissue morphology also suggests that the technique has the potential to improve tumor detection, at least in those tumors with higher levels of lactate labeling. A similar observation was made in a clinical study in the

prostate, where lactate labeling was observed in tumor tissue that was not detectable in a T_2-weighted ^{1}H image (13).

Although lactate labeling levels were relatively low we nevertheless observed consistent differences between the different models, which could not be explained by differences in PI3K/Akt pathway activity but which were correlated with the levels of c-Myc, LDHA, HK2, and plasma membrane localization of MCT1 and MCT4. The role of c-Myc in determining tumor lactate labeling, by driving increased expression of HK2 and LDHA, was confirmed by knocking down c-Myc expression in GB4 tumors. This reduced the expression of LDHA and HK2 and decreased lactate labeling. The levels of c-Myc in GB appear to be upregulated by two complementary mechanisms: alternative splicing of Delta Max (44) and mTORC2-dependent phosphorylation and inhibition of HDACs, leading to acetylation and inactivation of FoxO and relief of mir-34c-dependent c-Myc suppression (38). In this latter study treatment of GB cells with PI3K or Akt inhibitors was shown to elevate c-Myc levels and increase the levels of LDHA and HK2. Consistent with these observations we observed a negative correlation between the levels of pAkt and lactate labeling. The patterns of c-Myc, HK2 and LDHA expression observed in the tumors *in vivo* were not entirely reproduced in the cells cultured *in vitro*. This effect of the tumor microenvironment on gene expression is consistent with a recent RNAi screen of epigenetic modifiers in GB (45), which showed very different results when cells were grown in culture or as orthotopic xenografts.

The expression of c-Myc (8,9) and plasma membrane localization of MCT1 and MCT4 (37) have been shown previously to correlate with tumor grade, increased HK2 expression has been correlated with worse overall survival (39) and ^{1}H MRS measurements have demonstrated higher lactate concentrations in grade III and IV tumors (46). Therefore ^{13}C MRSI measurements of GB lactate labeling could provide prognostic information in the clinic. Moreover, since therapeutic resistance to PI3K or Akt inhibition is mediated by sustained c-Myc activity (38) the technique should also be capable of early detection of drug resistance and response to drugs that modulate c-Myc expression (38,47). The technique could potentially be used to select patients for metabolic therapies, for example drugs that target increased c-Myc driven glycolysis, such as the nicotinamide phosphoribosyl-transferase inhibitor (NAMPT), which has demonstrated efficacy in c-Myc-driven GB cells and in patient-derived orthotopic GB xenografts (48).

Detection of response to radiotherapy has been shown previously in a rat cell line glioma model (C6) (25), where response was evident as a decrease in lactate labeling. We have demonstrated here in GB4 tumors, which like C6 tumors show high levels of lactate labeling, that response to concomitant Temozolomide and radiation treatment results in decreased in lactate labeling, which was explained by increased levels of cell death. However, detection of response using this technique in those tumors that show much lower levels of lactate labeling may be challenging as the decrease in lactate labeling post treatment would necessarily be less.

Inhibition of LDHA (41) or HK2 (39) has been shown to sensitize GB cells to radiotherapy and we have shown that c-Myc and glycolytic enzyme expression are correlated with the radio-resistance of the cell lines *in vitro*. Therefore imaging with hyperpolarized [1-^{13}C]pyruvate could potentially be used clinically to target increased radiotherapy dose to radio-resistant tumors or specific regions of tumors i.e. regions that display increased lactate labeling. PET with ^{11}C methionine, where the resolution was 4.8 mm, has been used to target radiotherapy in glioblastoma patients (49). Since the resolution in the first clinical studies with hyperpolarized [1-^{13}C]pyruvate in prostate was between 7 and 15 mm (13) this suggests that the technique may have sufficient spatial resolution to do this.

In summary, increased levels of lactate labeling in GB PDOX models can be explained by increased levels of LDHA, HK2 and plasma membrane MCTs resulting from increased c-Myc expression. With the recent translation of this technique to the clinic, metabolic imaging with hyperpolarized [1-^{13}C]pyruvate could be used clinically for determining disease prognosis, for assessing response to drugs that are effective in reducing the levels of c-Myc and inducing cell death and for targeting radiation at tumor regions with high c-Myc expression and which are expected to be radio-resistant.

Acknowledgements:

The authors acknowledge the support of the Cancer Research UK Cambridge Institute core facilities, in particular the biological resources unit, genomics, bioinformatics, histopathology and pre-clinical imaging sections. We would

like to thank also Ms Leigh-Anne McDuffus, Ms Jodi Miller, Ms Bev Wilson, Mr Mike Mitchell, Mr Matt Clayton, Mr Ian Hall, Dr Jane Gray and Mr Ashley Sawle.

Data availability. Raw data associated with the figures can be accessed at: https://www.repository.cam.ac.uk/XXXX

References

1. Ostrom QT, Gittleman H, Fulop J, Liu M, Blanda R, Kromer C*, et al.* CBTRUS Statistical Report: Primary Brain and Central Nervous System Tumors Diagnosed in the United States in 2008-2012. Neuro Oncol **2015**;17 Suppl 4:iv1-iv62
2. Huse JT, Phillips HS, Brennan CW. Molecular subclassification of diffuse gliomas: seeing order in the chaos. Glia **2011**;59:1190-9
3. Stupp R, Hegi ME, Mason WP, van den Bent MJ, Taphoorn MJ, Janzer RC*, et al.* Effects of radiotherapy with concomitant and adjuvant temozolomide versus radiotherapy alone on survival in glioblastoma in a randomised phase III study: 5-year analysis of the EORTC-NCIC trial. Lancet Oncol **2009**;10:459-66
4. Wen PY, Kesari S. Malignant gliomas in adults. N Engl J Med **2008**;359:492-507
5. The Cancer Genome Atlas Research N. Comprehensive genomic characterization defines human glioblastoma genes and core pathways. Nature **2008**;455:1061-8
6. Ward PS, Thompson CB. Metabolic Reprogramming: A Cancer Hallmark Even Warburg Did Not Anticipate. Cancer Cell **2012**;21:297-308
7. Rodon J, Dienstmann R, Serra V, Tabernero J. Development of PI3K inhibitors: lessons learned from early clinical trials. Nat Rev Clin Oncol **2013**;10:143-53
8. Orian JM, Vasilopoulos K, Yoshida S, Kaye AH, Chow CW, Gonzales MF. Overexpression of multiple oncogenes related to histological grade of astrocytic glioma. British Journal of Cancer **1992**;66:106-12
9. Herms JW, von Loewenich FD, Behnke J, Markakis E, Kretzschmar HA. c-myc oncogene family expression in glioblastoma and survival. Surg Neurol **1999**;51:536-42
10. Stine ZE, Walton ZE, Altman BJ, Hsieh AL, Dang CV. MYC, Metabolism, and Cancer. Cancer Discovery **2015**;5:1024-39
11. Ardenkjaer-Larsen JH, Fridlund B, Gram A, Hansson G, Hansson L, Lerche MH*, et al.* Increase in signal-to-noise ratio of > 10,000 times in liquid-state NMR. Proc Natl Acad Sci U S A **2003**;100:10158-63

12. Brindle KM. Imaging metabolism with hyperpolarized (13)C-labeled cell substrates. J Am Chem Soc **2015**;137:6418-27
13. Nelson SJ, Kurhanewicz J, Vigneron DB, Larson PE, Harzstark AL, Ferrone M*, et al.* Metabolic imaging of patients with prostate cancer using hyperpolarized [1-^{13}C]pyruvate. Sci Transl Med **2013**;5:198ra08
14. Najac C, Ronen SM. MR Molecular Imaging of Brain Cancer Metabolism Using Hyperpolarized 13C Magnetic Resonance Spectroscopy. Top Magn Reson Imaging **2016**;25:187-96
15. Lee J, Kotliarova S, Kotliarov Y, Li A, Su Q, Donin NM*, et al.* Tumor stem cells derived from glioblastomas cultured in bFGF and EGF more closely mirror the phenotype and genotype of primary tumors than do serum-cultured cell lines. Cancer Cell **2006**;9:391-403
16. Wakimoto H, Mohapatra G, Kanai R, Curry WT, Jr., Yip S, Nitta M*, et al.* Maintenance of primary tumor phenotype and genotype in glioblastoma stem cells. Neuro Oncol **2012**;14:132-44
17. Stummer W, Pichlmeier U, Meinel T, Wiestler OD, Zanella F, Reulen HJ. Fluorescence-guided surgery with 5-aminolevulinic acid for resection of malignant glioma: a randomised controlled multicentre phase III trial. Lancet Oncol **2006**;7:392-401
18. Piccirillo SG, Dietz S, Madhu B, Griffiths J, Price SJ, Collins VP*, et al.* Fluorescence-guided surgical sampling of glioblastoma identifies phenotypically distinct tumour-initiating cell populations in the tumour mass and margin. Br J Cancer **2012**;107:462-8
19. Wiederschain D, Wee S, Chen L, Loo A, Yang G, Huang A*, et al.* Single-vector inducible lentiviral RNAi system for oncology target validation. Cell Cycle **2009**;8:498-504
20. Wee S, Wiederschain D, Maira S-M, Loo A, Miller C, deBeaumont R*, et al.* PTEN-deficient cancers depend on PIK3CB. Proceedings of the National Academy of Sciences of the United States of America **2008**;105:13057-62
21. Zufferey R, Nagy D, Mandel RJ, Naldini L, Trono D. Multiply attenuated lentiviral vector achieves efficient gene delivery in vivo. Nat Biotechnol **1997**;15:871-5
22. Garwood M, DelaBarre L. The return of the frequency sweep: designing adiabatic pulses for contemporary NMR. J Magn Reson **2001**;153:155-77
23. Tkac I, Starcuk Z, Choi IY, Gruetter R. In vivo 1H NMR spectroscopy of rat brain at 1 ms echo time. Magn Reson Med **1999**;41:649-56
24. Pfeuffer J, Tkac I, Provencher SW, Gruetter R. Toward an in vivo neurochemical profile: quantification of 18 metabolites in short-echo-time (1)H NMR spectra of the rat brain. J Magn Reson **1999**;141:104-20
25. Day SE, Kettunen MI, Cherukuri MK, Mitchell JB, Lizak MJ, Morris HD*, et al.* Detecting response of rat C6 glioma tumors to radiotherapy using hyperpolarized [1- 13C]pyruvate and 13C magnetic resonance spectroscopic imaging. Magn Reson Med **2011**;65:557-63
26. Li H, Durbin R. Fast and accurate short read alignment with Burrows-Wheeler transform. Bioinformatics **2009**;25:1754-60
27. McKenna A, Hanna M, Banks E, Sivachenko A, Cibulskis K, Kernytsky A*, et al.* The Genome Analysis Toolkit: A MapReduce framework for

analyzing next-generation DNA sequencing data. Genome Research **2010**;20:1297-303
28. Wang K, Li M, Hakonarson H. ANNOVAR: functional annotation of genetic variants from high-throughput sequencing data. Nucleic Acids Res **2010**;38:e164
29. Ramos AH, Lichtenstein L, Gupta M, Lawrence MS, Pugh TJ, Saksena G*, et al.* Oncotator: cancer variant annotation tool. Hum Mutat **2015**;36:E2423-9
30. Patil V, Pal J, Somasundaram K. Elucidating the cancer-specific genetic alteration spectrum of glioblastoma derived cell lines from whole exome and RNA sequencing. Oncotarget **2015**;6:43452-71
31. Yung WK, Luna M, Borit A. Vimentin and glial fibrillary acidic protein in human brain tumors. J Neurooncol **1985**;3:35-8
32. Mizoguchi M, Nutt CL, Mohapatra G, Louis DN. Genetic alterations of phosphoinositide 3-kinase subunit genes in human glioblastomas. Brain Pathol **2004**;14:372-7
33. Radoul M, Chaumeil MM, Eriksson P, Wang AS, Phillips JJ, Ronen SM. MR Studies of Glioblastoma Models Treated with Dual PI3K/mTOR Inhibitor and Temozolomide:Metabolic Changes Are Associated with Enhanced Survival. Mol Cancer Ther **2016**;15:1113-22
34. Reynolds S, Metcalf S, Cochrane EJ, Collins RC, Jones S, Paley MNJ*, et al.* Direct arterial injection of hyperpolarized 13C-labeled substrates into rat tumors for rapid MR detection of metabolism with minimal substrate dilution. Magnetic Resonance in Medicine **2017**;78:2116-26
35. Witney TH, Kettunen MI, Brindle KM. Kinetic modeling of hyperpolarized 13C label exchange between pyruvate and lactate in tumor cells. J Biol Chem **2011**;286:24572-80
36. Harris T, Eliyahu G, Frydman L, Degani H. Kinetics of hyperpolarized 13C1-pyruvate transport and metabolism in living human breast cancer cells. Proc Natl Acad Sci U S A **2009**;106:18131-6
37. Miranda-Goncalves V, Honavar M, Pinheiro C, Martinho O, Pires MM, Pinheiro C*, et al.* Monocarboxylate transporters (MCTs) in gliomas: expression and exploitation as therapeutic targets. Neuro Oncol **2013**;15:172-88
38. Masui K, Tanaka K, Akhavan D, Babic I, Gini B, Matsutani T*, et al.* mTOR complex 2 controls glycolytic metabolism in glioblastoma through FoxO acetylation and upregulation of c-Myc. Cell Metab **2013**;18:726-39
39. Wolf A, Agnihotri S, Micallef J, Mukherjee J, Sabha N, Cairns R*, et al.* Hexokinase 2 is a key mediator of aerobic glycolysis and promotes tumor growth in human glioblastoma multiforme. J Exp Med **2011**;208:313-26
40. Sottoriva A, Spiteri I, Piccirillo SG, Touloumis A, Collins VP, Marioni JC*, et al.* Intratumor heterogeneity in human glioblastoma reflects cancer evolutionary dynamics. Proc Natl Acad Sci U S A **2013**;110:4009-14
41. Koukourakis M, Tsolou A, Pouliliou S, Lamprou I, Papadopoulou M, Ilemosoglou M*, et al.* Blocking LDHA glycolytic pathway sensitizes glioblastoma cells to radiation and temozolomide. Biochem Biophys Res Commun **2017**;491:932-8

42. Maher EA, Marin-Valencia I, Bachoo RM, Mashimo T, Raisanen J, Hatanpaa KJ*, et al.* Metabolism of [U-(13)C]glucose in Human Brain Tumors In Vivo. NMR in biomedicine **2012**;25:1234-44
43. Marin-Valencia I, Yang C, Mashimo T, Cho S, Baek H, Yang XL*, et al.* Analysis of tumor metabolism reveals mitochondrial glucose oxidation in genetically diverse human glioblastomas in the mouse brain in vivo. Cell Metab **2012**;15:827-37
44. Babic I, Anderson ES, Tanaka K, Guo D, Masui K, Li B*, et al.* EGFR mutation-induced alternative splicing of Max contributes to growth of glycolytic tumors in brain cancer. Cell Metab **2013**;17:1000-8
45. Miller TE, Liau BB, Wallace LC, Morton AR, Xie Q, Dixit D*, et al.* Transcription elongation factors represent in vivo cancer dependencies in glioblastoma. Nature **2017**;547:355-9
46. Chang SM, Nelson S, Vandenberg S, Cha S, Prados M, Butowski N*, et al.* Integration of preoperative anatomic and metabolic physiologic imaging of newly diagnosed glioma. Journal of Neuro-Oncology **2009**;92:401
47. Annibali D, Whitfield JR, Favuzzi E, Jauset T, Serrano E, Cuartas I*, et al.* Myc inhibition is effective against glioma and reveals a role for Myc in proficient mitosis. Nat Commun **2014**;5:4632
48. Tateishi K, Iafrate AJ, Ho Q, Curry WT, Batchelor TT, Flaherty KT*, et al.* Myc-Driven Glycolysis Is a Therapeutic Target in Glioblastoma. Clin Cancer Res **2016**;22:4452-65
49. Miwa K, Matsuo M, Ogawa S-i, Shinoda J, Yokoyama K, Yamada J*, et al.* Re-irradiation of recurrent glioblastoma multiforme using ^{11}C-methionine PET/CT/MRI image fusion for hypofractionated stereotactic radiotherapy by intensity modulated radiation therapy. Radiation Oncology (London, England) **2014**;9:181

Figure legends

Figure 1 Patient-derived orthotopic xenografts (PDOX) resemble human glioblastoma and show increased hyperpolarized [1-^{13}C]lactate/[1-^{13}C]pyruvate signal ratios when compared with normal brain tissue. a) Time taken from cell implantation for tumors to reach >0.05 cm^3. (GB1 n=9, GB2 n=7, GB3 n=5, GB4 n=21, U87 n=14, p<0.0001). All of the cell lines showed high levels of tumor initiation and growth following orthotopic cell implantation (GB1, 9 tumors from 9 implantations; GB2 9/9, GB3 5/6, GB4 23/25). b) Percentage of cells showing immunostaining for

GFAP in the PDOX and U87 tumor models (GB1 n=7, GB2 n=5, GB3 n=2, GB4 n=19, U87 n=8). (c) Western blot of nestin expression in the indicated cell lines in vitro. Representative false color images of the hyperpolarized [1-^{13}C]lactate/[1-^{13}C]pyruvate signal ratio (LPR) superimposed on a T_2-weighted ^{1}H image (grayscale) of (d) a control brain (no implanted tumor cells) and (e) a brain one month after implantation of GB4 cells (the site of implantation is arrowed). The scale bar indicates LPR. Representative T_2-weighted image (j) and T_1–weighted ^{1}H images before (k) and after (l) contrast agent injection and one month after GB4 cell implantation (the site of implantation is arrowed). f) LPRs averaged over the hemispheres containing implanted cells (right) and non-implanted (left) one month after GB4 cell implantation. The ratio was significantly higher in the right hemisphere (*p=0.02, n=11, paired t-test). g) LPRs in control brains, which showed no significant difference between the hemispheres (p=0.9, n=6, paired t-test). LPRs averaged over the lower (h) and upper (i) quadrants of the indicated hemispheres one month after GB4 cell implantation in the right lower brain quadrant. There was a significant increase in the quadrant containing implanted cells (right) (*p=0.01, n=11, paired t-test) but no significant difference between the upper quadrants (p=0.3, n=11, paired t-test).

Figure 2 The different tumor models showed differences in hyperpolarized [1-^{13}C]lactate/[1-^{13}C]pyruvate signal ratios Representative false color images of the hyperpolarized [1-^{13}C]lactate/ [1-^{13}C]pyruvate signal ratio (LPR) superimposed on T_2-weighted ^{1}H images (grayscale) from animals implanted with (a) GB1 cells; (b) GB2 cells; (c) GB3 cells; (d) GB4 cells; (e)

U87 cells. Spectra from representative voxels are also shown. f) LPRs in tumors resulting from implantation of the indicated cell lines. Controls were not implanted with cells. (**p<0.009, ***p<0.0004, **** p<0.0001. (Control n=6, GB1 n=5, GB2 n=9, GB3 n=3, GB4 n=12, U87 n=10, unpaired t-test). Images were acquired at the following times after cell implantation; GB1, 153 days; GB2, 322 days; GB3, 163 days; GB4, 121 days; U87, 27 days.

Figure 3 Expression of c-Myc, LDH A and HK2 and MCT plasma membrane localisation are correlated with the hyperpolarized [1-^{13}C]lactate/[1-^{13}C]pyruvate signal ratio Western blot analysis of the expression of c-Myc (a), LDHA (b), and HK2 (c) in the indicated tumor models. d) Immunohistochemical staining of c-Myc in the indicated tumor models and quantitative analysis of these data (e) (**p=0.009, n=2-5, unpaired t-test). Expression of c-Myc (f), LDHA (g) and HK2 (h) in the corresponding cell lines cultured in vitro (*p<0.05, **p<0.007, ***p<0.0005, unpaired t-test). For c-Myc there were three biological replicates and for LDHA and HK2 two, and two technical replicates for each sample. Band intensities were normalized to that for β-actin. i) Immunohistochemical analysis of MCT1 and MCT4 expression in the indicated tumor models; plasma membrane localisation is evident in GB3 and GB4 tumors. Correlations between LPRs measured in vivo and c-Myc expression (r^2 = 0.83, **p=0.002, n=4, linear regression) (j) and phosphorylated Akt (pAKT) (r^2 = 0.76, **p=0.005, n=4, linear regression) (k), determined by western blotting, in the indicated tumor models.

Figure 4 Inhibition of c-Myc expression decreased the hyperpolarized [1-^{13}C]lactate/[1-^{13}C]pyruvate signal ratio and increased radiosensitivity Expression of c-Myc, LDHA and HK2 (a – c) (normalized to β-actin) 48 h after addition of doxycycline (dox) to GB4 c-Myc KD cells. There were two biological replicates and two technical replicates per sample (*p<0.05, unpaired t-test). d) Change in the hyperpolarized [1-^{13}C]lactate/[1-^{13}C]pyruvate signal ratios (LPRs) in tumors resulting from orthotopic implantation of GB4 c-Myc KD and GB4 cells one week after addition of doxycycline to the diet (*p=0.035, n=3, paired t-test). LPR images, superimposed on grayscale ^{1}H images, of a GB4 c-Myc KD tumor-bearing rat prior to (e) and after (f) addition of doxycycline to the diet. g) Response of GB4 and GB1 cells to 15 Gy radiation at day 0. (P<0.0001; 2 biological replicates, 50 technical replicates, unpaired t-test). Viability is shown as the percentage of viable cells determined using an automated Trypan blue dye exclusion assay, as described in the methods section. h) GB4 c-Myc KD cells cultured with doxycycline for 48 h prior to radiation with 15 Gy showed a significant increase in the loss of cell viability (P=0.008; 4 biological replicates, 50 technical replicates, unpaired t-test). There was no significant difference in the change in viability following irradiation of GB4 cells and GB4 cells expressing a control shRNA between those cells that had previously been incubated with doxycycline and those that had not (Suppl. Fig. 5). LPR images superimposed on ^{1}H images of a GB4 tumor prior to (i) and after (j) treatment with Temozolomide and 40 Gy of radiation. k) LPRs at 72 h after treatment with Temozolomide and 40 Gy of radiation (*p=0.038 n=6, paired t-test). l) TUNEL staining of untreated tumors and tumors 72 h after treatment

with Temozolomide and 40 Gy of radiation (**p<0.0089, n=11 untreated, n=8 treated, unpaired t-test).

Figure 1

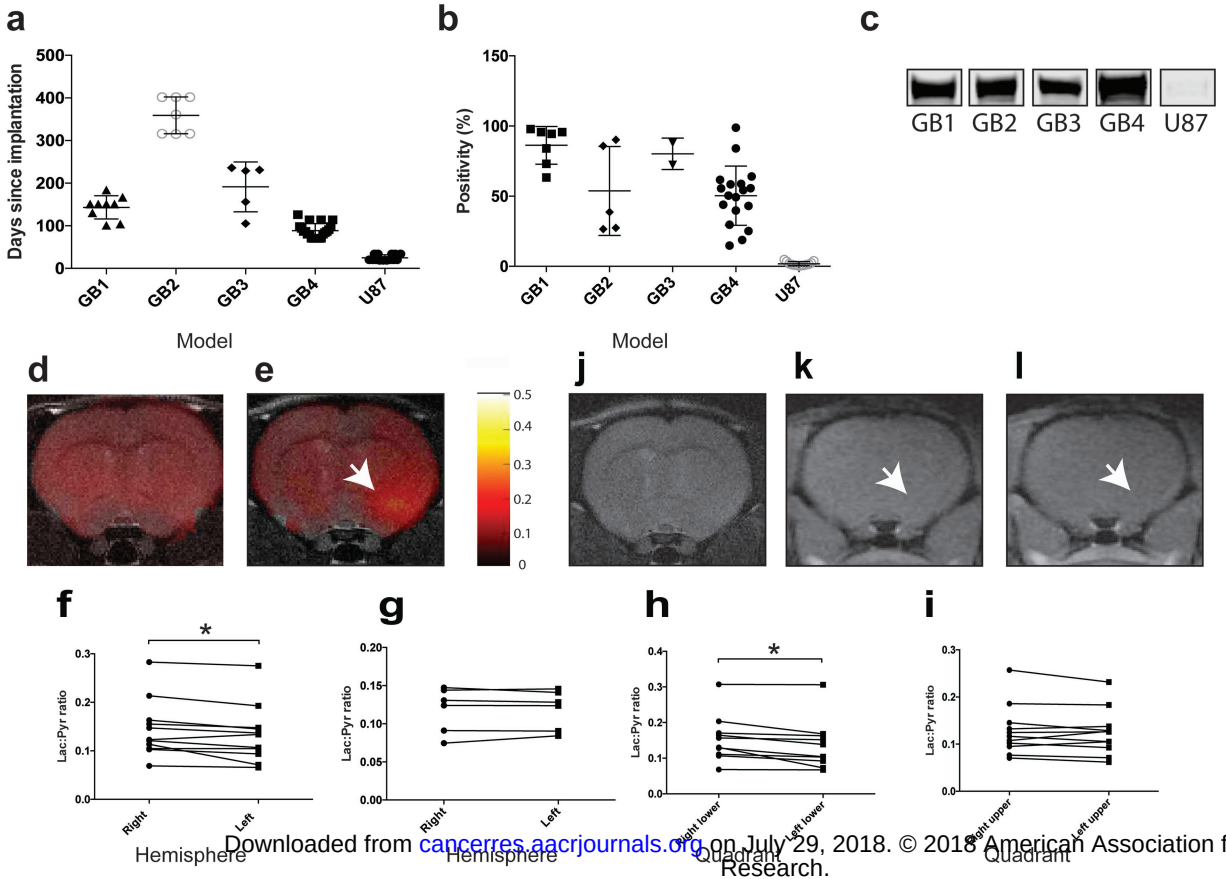

Figure 2

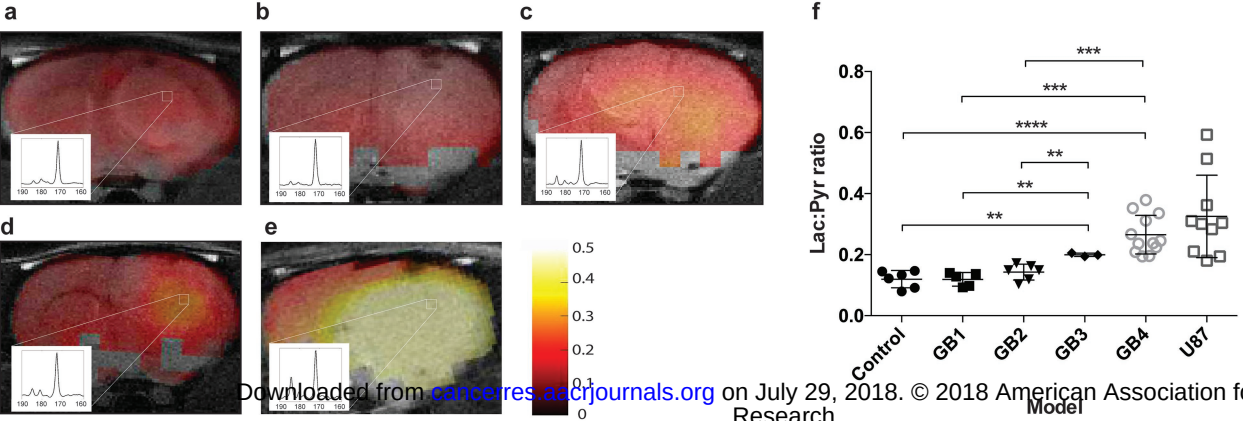

Figure 3

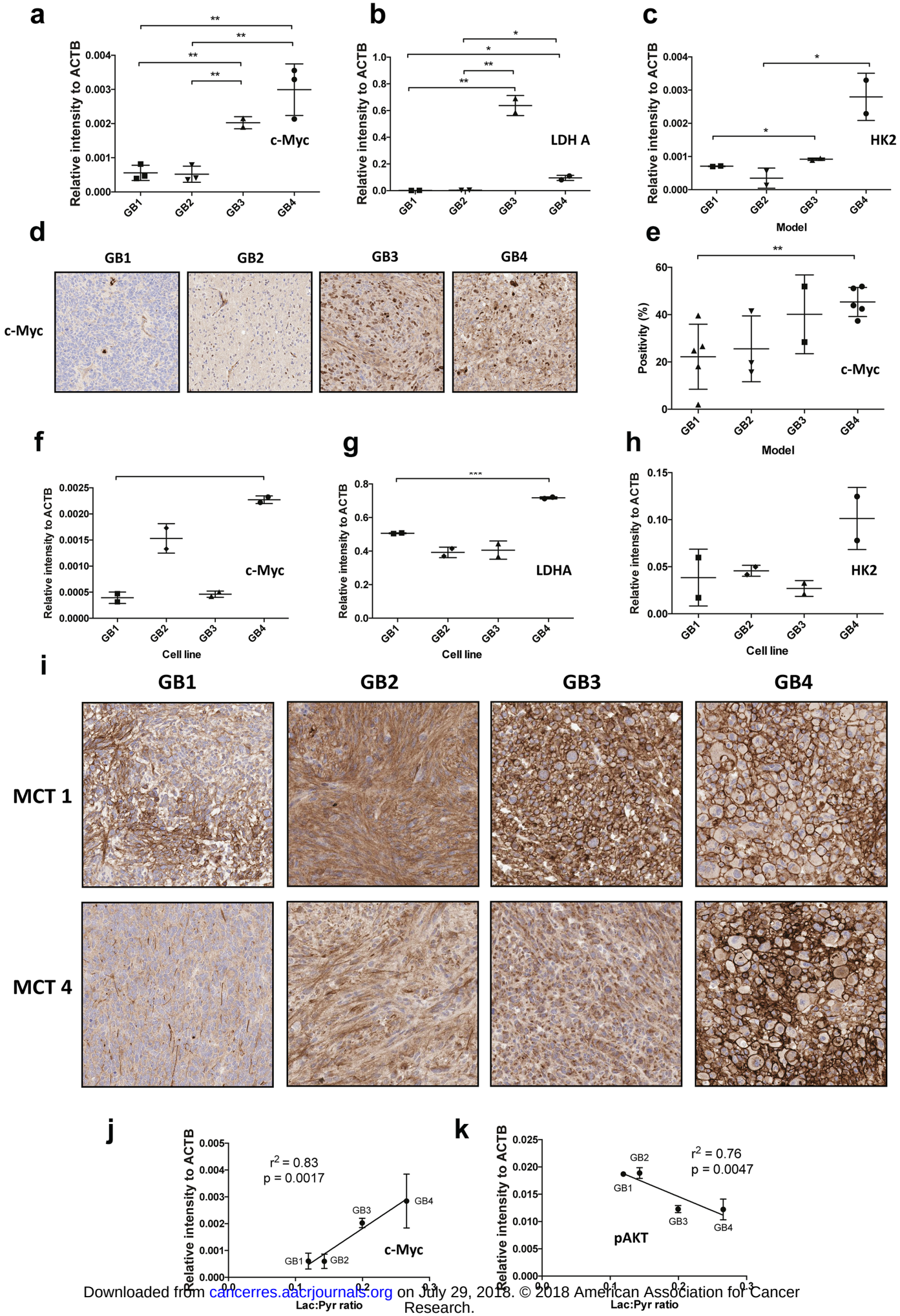

Figure 4

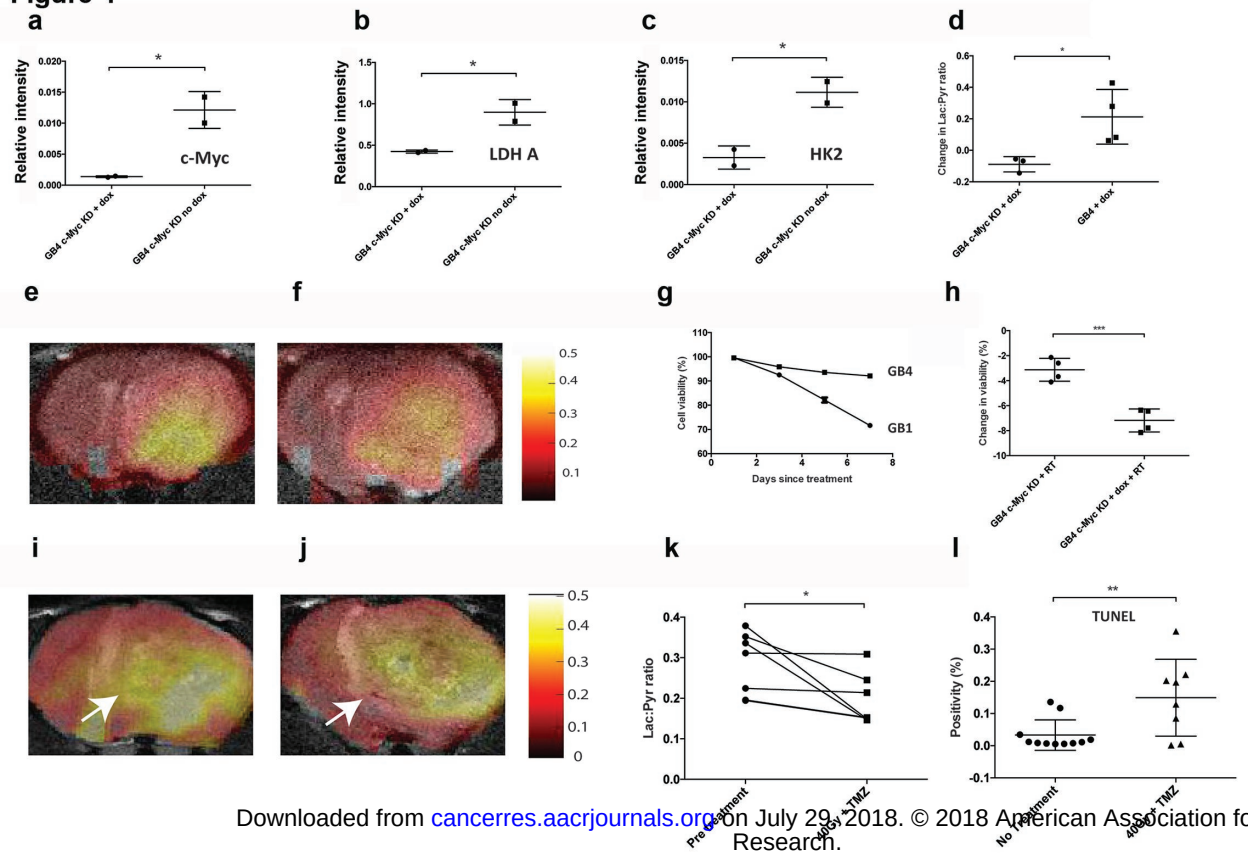

AACR American Association for Cancer Research

Cancer Research

The Journal of Cancer Research (1916–1930) | The American Journal of Cancer (1931–1940)

Metabolic imaging detects low levels of glycolytic activity that vary with levels of c-Myc expression in patient-derived xenograft models of glioblastoma

Richard Mair, Alan Wright, Susana Ros, et al.

Cancer Res Published OnlineFirst July 27, 2018.